

Multiple generations of high-order orbital angular momentum modes through cascaded third-harmonic generation in a 2D nonlinear photonic crystal

DAN WEI,¹ JIALE GUO,¹ XINYUAN FANG,¹ DUNZHAO WEI,¹ RUI NI,¹ PENG CHEN,¹ XIAOPENG HU,¹ YONG ZHANG,^{1,*} WEI HU,¹ Y. Q. LU,¹ S. N. ZHU,¹ AND MIN XIAO^{1,2}

¹National Laboratory of Solid State Microstructures, College of Engineering and Applied Sciences and School of Physics, Nanjing University, Nanjing 210093, China

²Department of Physics, University of Arkansas, Fayetteville, Arkansas 72701, USA

*zhangyong@nju.edu.cn

Abstract: We experimentally demonstrate multiple generations of high-order orbital angular momentum (OAM) modes through third-harmonic generation in a 2D nonlinear photonic crystal. Such third-harmonic generation process is achieved by cascading second-harmonic generation and sum-frequency generation using the non-collinear quasi-phase-matching technique. This technique allows multiple OAM modes with different colors to be simultaneously generated. Moreover, the OAM conservation law guarantees that the topological charge is tripled in the cascaded third-harmonic generation process. Our method is effective for obtaining multiple high-order OAM modes for optical imaging, manipulation, and communications.

©2017 Optical Society of America

OCIS codes: (050.4865) Optical vortices; (190.0190) Nonlinear optics; (190.4160) Multiharmonic generation.

References and links

1. W. P. Schleich, "Quantum optics: optical coherence and quantum optics," *Science* **272**(5270), 1897–1898 (1996).
2. G. C. Hegerfeldt, "Photons and atoms—introduction to quantum electrodynamics," *Science* **247**(4943), 732–733 (1990).
3. L. Allen, M. W. Beijersbergen, R. J. C. Spreeuw, and J. P. Woerdman, "Orbital angular momentum of light and the transformation of Laguerre-Gaussian laser modes," *Phys. Rev. A* **45**(11), 8185–8189 (1992).
4. D. McGloin, V. Garcés-Chávez, and K. Dholakia, "Interfering Bessel beams for optical micromanipulation," *Opt. Lett.* **28**(8), 657–659 (2003).
5. L. Paterson, M. P. MacDonald, J. Arlt, W. Sibbett, P. E. Bryant, and K. Dholakia, "Controlled rotation of optically trapped microscopic particles," *Science* **292**(5518), 912–914 (2001).
6. K. Dholakia and T. Cizmar, "Shaping the future of manipulation," *Nat. Photonics* **5**(6), 335–342 (2011).
7. H. I. Sztul and R. R. Alfano, "Double-slit interference with Laguerre-Gaussian beams," *Opt. Lett.* **31**(7), 999–1001 (2006).
8. V. D'Ambrosio, N. Spagnolo, L. Del Re, S. Slussarenko, Y. Li, L. C. Kwek, L. Marrucci, S. P. Walborn, L. Aolita, and F. Sciarrino, "Photonic polarization gears for ultra-sensitive angular measurements," *Nat. Commun.* **4**(9), 2432 (2013).
9. G. Gibson, J. Courtial, M. Padgett, M. Vasnetsov, V. Pas'ko, S. Barnett, and S. Franke-Arnold, "Free-space information transfer using light beams carrying orbital angular momentum," *Opt. Express* **12**(22), 5448–5456 (2004).
10. J. Wang, J. Y. Yang, I. M. Fazal, N. Ahmed, Y. Yan, H. Huang, Y. X. Ren, Y. Yue, S. Dolinar, M. Tur, and A. E. Willner, "Terabit free-space data transmission employing orbital angular momentum multiplexing," *Nat. Photonics* **6**(7), 488–496 (2012).
11. N. Bozinovic, Y. Yue, Y. Ren, M. Tur, P. Kristensen, H. Huang, A. E. Willner, and S. Ramachandran, "Terabit-scale orbital angular momentum mode division multiplexing in fibers," *Science* **340**(6140), 1545–1548 (2013).
12. A. Mair, A. Vaziri, G. Weihs, and A. Zeilinger, "Entanglement of the orbital angular momentum states of photons," *Nature* **412**(6844), 313–316 (2001).
13. A. C. Dada, J. Leach, G. S. Buller, M. J. Padgett, and E. Andersson, "Experimental high-dimensional two-photon entanglement and violations of generalized Bell inequalities," *Nat. Phys.* **7**(9), 677–680 (2011).

14. J. T. Barreiro, T. C. Wei, and P. G. Kwiat, "Beating the channel capacity limit for linear photonic superdense coding," *Nat. Phys.* **4**(4), 282–286 (2008).
15. L. Marrucci, L. C. Manzo, and D. Paparo, "Optical spin-to-orbital angular momentum conversion in inhomogeneous anisotropic media," *Phys. Rev. Lett.* **6**(16), 163905 (2006).
16. M. J. Tang, P. Chen, W. L. Zhang, A. M. Tam, V. G. Chigrinov, W. Hu, and Y. Q. Lu, "Integrated and reconfigurable optical paths based on stacking optical functional films," *Opt. Express* **24**(22), 25510–25514 (2016).
17. R. K. Tyson, M. Scipioni, and J. Viegas, "Generation of an optical vortex with a segmented deformable mirror," *Appl. Opt.* **47**(33), 6300–6306 (2008).
18. N. R. Heckenberg, R. McDuff, C. P. Smith, and A. G. White, "Generation of optical phase singularities by computer-generated holograms," *Opt. Lett.* **17**(3), 221–223 (1992).
19. M. W. Beijersbergen, R. P. C. Coerwinkel, M. Kristensen, and J. P. Woerdman, "Helical-wavefront laser beams produced with a spiral phaseplate," *Opt. Commun.* **112**(5–6), 321–327 (1994).
20. F. Bouchard, H. Larocque, A. M. Yao, C. Travis, I. De Leon, A. Rubano, E. Karimi, G. L. Oppo, and R. W. Boyd, "Polarization Shaping for Control of Nonlinear Propagation," *Phys. Rev. Lett.* **117**(23), 233903 (2016).
21. P. Chen, W. Ji, B. Y. Wei, W. Hu, V. Chigrinov, and Y. Q. Lu, "Generation of arbitrary vector beams with liquid crystal polarization converters and vector-photoaligned q-plates," *Appl. Phys. Lett.* **107**(24), 241102 (2015).
22. K. Dholakia, N. B. Simpson, M. J. Padgett, and L. Allen, "Second-harmonic generation and the orbital angular momentum of light," *Phys. Rev. A* **54**(5), R3742–R3745 (1996).
23. J. Arlt, K. Dholakia, L. Allen, and M. J. Padgett, "Parametric down-conversion for light beams possessing orbital angular momentum," *Phys. Rev. A* **59**(5), 3950–3952 (1999).
24. X. Y. Fang, D. Z. Wei, D. M. Liu, W. H. Zhong, R. Ni, Z. H. Chen, X. P. Hu, Y. Zhang, S. N. Zhu, and M. Xiao, "Multiple copies of orbital angular momentum states through second-harmonic generation in a two-dimensional periodically poled LiTO₃," *Appl. Phys. Lett.* **107**(16), 161102 (2015).
25. X. Fang, G. Yang, D. Wei, D. Wei, R. Ni, W. Ji, Y. Zhang, X. Hu, W. Hu, Y. Q. Lu, S. N. Zhu, and M. Xiao, "Coupled orbital angular momentum conversions in a quasi-periodically poled LiTaO₃ crystal," *Opt. Lett.* **41**(6), 1169–1172 (2016).
26. A. Beržanskis, A. Matijosius, A. Piskarskas, V. Smilgevičius, and A. Stabinis, "Sum-frequency mixing of optical vortices in nonlinear crystals," *Opt. Commun.* **150**(1–6), 372–380 (1998).
27. G. H. Shao, Z. J. Wu, J. H. Chen, F. Xu, and Y. Q. Lu, "Nonlinear frequency conversion of fields with orbital angular momentum using quasi-phase-matching," *Phys. Rev. A* **88**(6), 063827 (2013).
28. R. Ni, Y. Niu, L. Du, X. P. Hu, Y. Zhang, and S. N. Zhu, "Topological charge transfer in frequency doubling of fractional orbital angular momentum state," *Appl. Phys. Lett.* **109**(15), 151103 (2016).
29. Y. M. Wang, D. Z. Wei, Y. Z. Zhu, X. Y. Huang, X. Y. Fang, W. H. Zhong, Q. J. Wang, Y. Zhang, and M. Xiao, "Conversion of the optical orbital angular momentum in a plasmon-assisted second-harmonic generation," *Appl. Phys. Lett.* **109**(8), 081105 (2016).
30. G. Gariepy, J. Leach, K. T. Kim, T. J. Hammond, E. Frumker, R. W. Boyd, and P. B. Corkum, "Creating high-harmonic beams with controlled orbital angular momentum," *Phys. Rev. Lett.* **113**(15), 153901 (2014).
31. V. Berger, "Nonlinear photonic crystals," *Phys. Rev. Lett.* **81**(19), 4136–4139 (1998).
32. Y. Zhang, J. Wen, S. N. Zhu, and M. Xiao, "Nonlinear Talbot effect," *Phys. Rev. Lett.* **104**(18), 183901 (2010).
33. P. Xu, S. H. Ji, S. N. Zhu, X. Q. Yu, J. Sun, H. T. Wang, J. L. He, Y. Y. Zhu, and N. B. Ming, "Conical second harmonic generation in a two-dimensional $\chi^{(2)}$ photonic crystal: a hexagonally poled LiTaO₃ crystal," *Phys. Rev. Lett.* **93**(13), 133904 (2004).
34. Y. Zhang, Z. Qi, W. Wang, and S. N. Zhu, "Quasi-phase-matched Cerenkov second-harmonic generation in a hexagonally poled LiTaO₃ waveguide," *Appl. Phys. Lett.* **89**(17), 171113 (2006).
35. Y. Zhang, Z. D. Gao, Z. Qi, S. N. Zhu, and N. B. Ming, "Nonlinear Cerenkov radiation in nonlinear photonic crystal waveguides," *Phys. Rev. Lett.* **100**(16), 163904 (2008).
36. A. Norton and C. de Sterke, "Two-dimensional poling patterns for 3rd and 4th harmonic generation," *Opt. Express* **11**(9), 1008–1014 (2003).
37. N. Fujioka, S. Ashihara, H. Ono, T. Shimura, and K. Kuroda, "Cascaded third-harmonic generation of ultrashort optical pulses in two-dimensional quasi-phase-matching gratings," *J. Opt. Soc. Am. B* **24**(9), 2394–2405 (2007).
38. W. Wang, V. Roppo, K. Kalinowski, Y. Kong, D. N. Neshev, C. Cojocaru, J. Trull, R. Vilaseca, K. Staliunas, W. Krolikowski, S. M. Saitiel, and Y. Kivshar, "Third-harmonic generation via broadband cascading in disordered quadratic nonlinear media," *Opt. Express* **17**(22), 20117–20123 (2009).
39. V. Denisenko, V. Shvedov, A. S. Desyatnikov, D. N. Neshev, W. Krolikowski, A. Volyar, M. Soskin, and Y. S. Kivshar, "Determination of topological charges of polychromatic optical vortices," *Opt. Express* **17**(26), 23374–23379 (2009).

1. Introduction

Angular momentum is one of the most important fundamental physical quantities in both classical and quantum mechanics [1], and can be divided into spin angular momentum (SAM) and orbital angular momentum (OAM) in paraxial beams [2]. SAM is associated with photon spin and OAM is linked to the spatial distribution of light. In 1992, Allen et al. reported that a

helically phased beam comprising an azimuthal phase term, $\exp(i l \phi)$, carries an OAM of $l \hbar$ per photon [3]. In contrast to the SAM, which has only two possible values of $\pm \hbar$, the theoretically unlimited values of l , in principle, provide an infinite range of achievable OAM states. High-order OAM modes are required in various applications, such as optical manipulation and trapping [4–6], high-precision optical measurements [7,8], high-capacity free space, fiber-optical communications [9–11], and in studies of fundamental quantum physics [12–14]. Various methods to imprint OAM onto light beams have been reported, including the use of Q-plates [15,16], segmented adaptive mirrors [17], holographic diffraction gratings [18], and a spiral phase plate [19]. However, it is generally difficult to produce a light beam carrying a high-order OAM using above methods. For example, because of the complex fabrication technology required, Q-plates with high topological charge have rarely been reported [20,21]. Recently, researchers introduced nonlinear optics to achieve high-order OAM-carrying light in nonlinear optical crystals [22–28], metasurfaces [29] and atomic vapor [30]. In these nonlinear processes, the total OAM conservation of all interactive lights plays a very important role in the generation of high-order OAM states. For example, in a second-harmonic generation (SHG) process, the topological charge of the second-harmonic wave can be twice that of the fundamental beam [24].

For nonlinear processes within crystals, quasi-phase matching (QPM) has the advantages of having effective nonlinear coefficients and no walk-off effect, in contrast to birefringence phase matching. Periodically poled crystals have been used to achieve efficient nonlinear conversion of OAM states through QPM [24,27]. In 1998, Berger et al. extended the QPM theory from 1D to 2D periodically poled nonlinear photonic crystals (NPCs) [31]. Various interesting phenomena have been demonstrated in 2D NPCs, such as nonlinear Talbot self-imaging [32], conical SHG beams [33], and nonlinear Cherenkov effect [34,35]. It is particularly noteworthy that cascaded nonlinear optical processes can also be efficiently realized in 2D NPCs. For example, third-harmonic generation (THG) was achieved through a cascade of SHG and sum-frequency generation (SFG) processes [36,37]. In addition, multiple cascaded nonlinear optical processes were shown to simultaneously take place at different directions through collinear and non-collinear reciprocal lattice vectors in a 2D NPC [38].

In this study, we report multiple generations of high-order OAM states through cascaded THG in a 2D NPC. The conservation law of OAM holds well in both the collinear and non-collinear cascaded THG processes. In the experiment, multiple blue OAM beams carrying a topological charge up to 12 were demonstrated. Higher topological charge can be achieved under our experimental configuration using cascaded high-harmonic generation. Our results may be useful for obtaining multiple high-order OAM modes for optical imaging, manipulation, and communications.

2. Experiment setup and theory

The sample in our experiment was a hexagonally poled LiTaO₃ crystal with a size of 10 mm (x) \times 4 mm (y) \times 0.5 mm (z), which was fabricated through a room-temperature electric-field poling technique. The period of the 2D structure was $d = 9.3 \mu\text{m}$, and the total inverted area was about 30% of the overall sample. To find possible phase-matching processes, we used the reciprocal lattice [Fig. 1(a)] formed by the fundamental vectors, \vec{e}_1 and \vec{e}_2 , between which the angle was 60° . The period of the reciprocal lattice was $4\pi / d\sqrt{3}$ and $e_1 = e_2 = 4\pi / d\sqrt{3}$. All other reciprocal vectors were found as $\vec{G}_{m,n} = m\vec{e}_1 + n\vec{e}_2$ with

$$G_{m,n} = \frac{4\pi\sqrt{m^2 + n^2 + mn}}{d\sqrt{3}}, \quad (1)$$

where the integers m and n represent the orders of the reciprocal vectors. Their directions can be collinear (for example, $\vec{G}_{1,0}$ in Fig. 1(a)) or non-collinear (for example, $\vec{G}_{0,1}, \vec{G}_{0,-1}, \vec{G}_{1,1}$ and $\vec{G}_{1,-1}$ in Fig. 1(a)).

A typical cascaded process in such a 2D NPC is THG, which can be achieved by cascading the SHG and SFG processes. Here, we assume that a fundamental beam with a frequency of ω_1 and an OAM of l_1 propagates along the \bar{y} direction of the 2D hexagonally poled LiTaO₃ crystal. The conservation of energy requires

$$\omega_2 = 2\omega_1, \quad (2)$$

$$\omega_3 = \omega_1 + \omega_2 = 3\omega_1. \quad (3)$$

Here, ω_2 and ω_3 are the frequencies of the second- and third-harmonic waves, respectively. The phase-matching condition can be written as

$$\Delta\vec{k}_1 = \vec{k}_{2\omega} - 2\vec{k}_\omega - \vec{G}_{m,n} = 0, \quad (4)$$

$$\Delta\vec{k}_2 = \vec{k}_{3\omega} - \vec{k}_{2\omega} - \vec{k}_\omega - \vec{G}_{m',n'} = 0, \quad (5)$$

where, \vec{k}_ω , $\vec{k}_{2\omega}$ and $\vec{k}_{3\omega}$ are the wave vectors of the fundamental, and second- and third-harmonic waves, respectively. In an ideal case with $\Delta\vec{k}_1 = \Delta\vec{k}_2 = 0$, one can achieve perfect phase-matching and high-efficiency SHG and THG. However, it is usually difficult in the experiment to satisfy $\Delta\vec{k}_1 = 0$ and $\Delta\vec{k}_2 = 0$ at the same time because of inaccurate refractive index used in designing the domain structure and fabrication errors. If $\Delta\vec{k}_1$ and $\Delta\vec{k}_2$ are close to 0, one can still enhance the conversion efficiency because the phase mismatch is partially compensated by the reciprocal vector in the PPLT crystal. In our experiment, the phase matching of the THG is achieved using $\vec{G}_{0,1}/\vec{G}_{0,-1}$ for SHG [Fig. 1(b)] and $\vec{G}_{1,1}/\vec{G}_{1,-1}$ for SFG [Fig. 1(c)]. The condition for OAM conservation can be written as

$$l_2 = 2l_1, \quad (6)$$

$$l_3 = l_1 + l_2 = 3l_1. \quad (7)$$

Here, l_2 and l_3 are the topological charges of the second- and third-harmonic OAM beams, respectively.

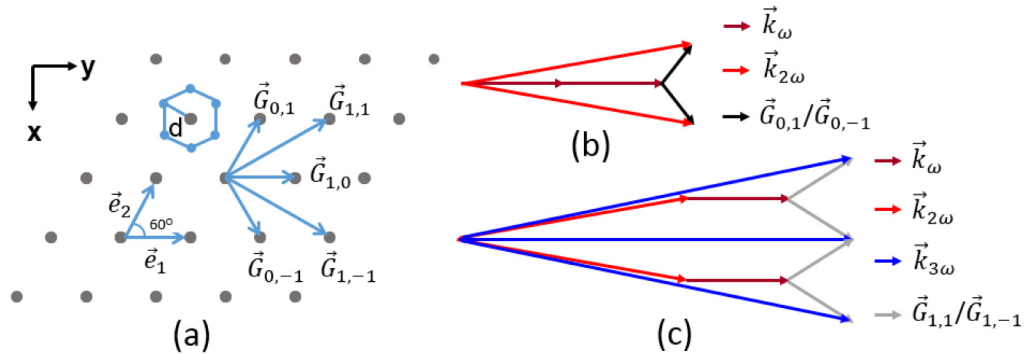


Fig. 1. (a) Schematic diagram of the reciprocal lattice for the 2D hexagonally poled LiTaO₃ crystal. In the experiments, the propagation of the fundamental beam was in the \bar{y} direction.

Note that the direction of \vec{y} is same as \vec{e}_1 . (b) QPM SHG with $\vec{G}_{0,1}$ and $\vec{G}_{0,-1}$. (c) QPM THG was achieved by cascading the SHG and SFG processes with $\vec{G}_{1,1}$ and $\vec{G}_{1,-1}$.

The experiment setup is shown in Fig. 2(a). The input fundamental field is generated by an optical parametric oscillator (Horizon 1-8572, Continuum Co.) pumped by a nanosecond laser system with a pulse width of about 6 ns and a repetition rate of 10 Hz. In the experiment, a Q-plate was used to imprint the OAM on the input fundamental beam, which was a half-wave plate fabricated by a birefringent liquid crystal with a space-variant optical axis in the transverse plane [21]. The geometry of the optical axis is defined by a topological charge ‘ q ’, which is an integer or semi-integer. When a circularly polarized light beam passes through such a Q-plate, an OAM of $2q$ is transferred into the beam. The first quarter-wave plate (QWP) was used to change the linear polarization (x axis) of the input fundamental light to a circular polarization. After passing the OAM information through the Q-plate, another QWP transforms the polarization back to a linear polarization along the z axis. Then, the fundamental wave with a known topological charge is focused onto the PPLT crystal along the y axis of the crystal. Under the experimental configuration, the nonlinear optical coefficient d_{33} of the LiTaO₃ crystal was utilized, which was periodically modulated in the hexagonally poled LiTaO₃ crystal. A cylindrical lens was used as a mode converter to analyze the OAM information from the SHG and THG patterns. By counting the dark strips in the converted pattern, one can obtain the topological charge of the OAM state [39].

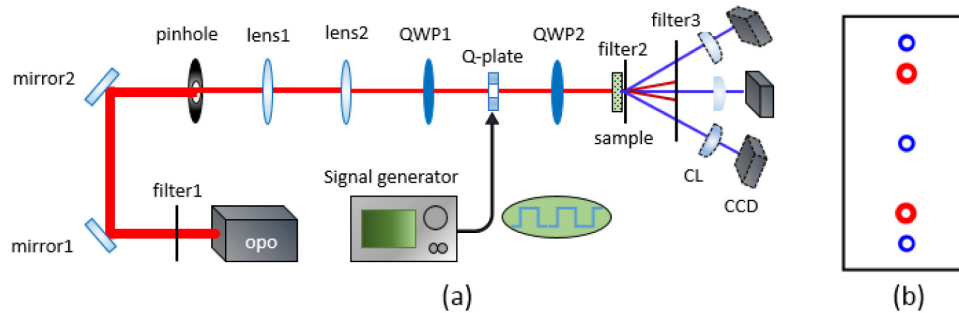


Fig. 2. (a) Schematic diagram of the experimental setup. (b) Distribution of the second and third harmonics on the screen. QWP: quarter wave plate; opo: optical parametric oscillator; CL: cylindrical lens.

3. Experiment result and discussion

In the experiment, the input fundamental beam was imprinted with an OAM of $l_1 = 1, 2, 3,$ or 4 . First, the input wavelength was set at 1362 nm. After filtering out the fundamental beam, the image of the SHG patterns was obtained, as shown in Fig. 3(a). The two second-harmonic rings result from the non-collinear SHG process, which is phase-matched by the reciprocal vectors $\vec{G}_{0,1}$ and $\vec{G}_{0,-1}$ [Fig. 1(b)]. Using the cylinder lens, the OAMs of the second-harmonic beam were $l_2 = 2, 4, 6,$ and 8 , which correspond to the input OAMs of $l_1 = 1, 2, 3,$ and 4 , respectively [Fig. 3(b)–(e)]. At this wavelength, the SHG is well phase-matched (i.e., $\Delta\vec{k}_1 = 0$); however, the QPM condition for the cascaded SFG process is not fulfilled (i.e., $\Delta\vec{k}_2$ is far from 0). Therefore, a clear third-harmonic OAM beam was not observed at this input wavelength, even when the efficiency of SHG was high.

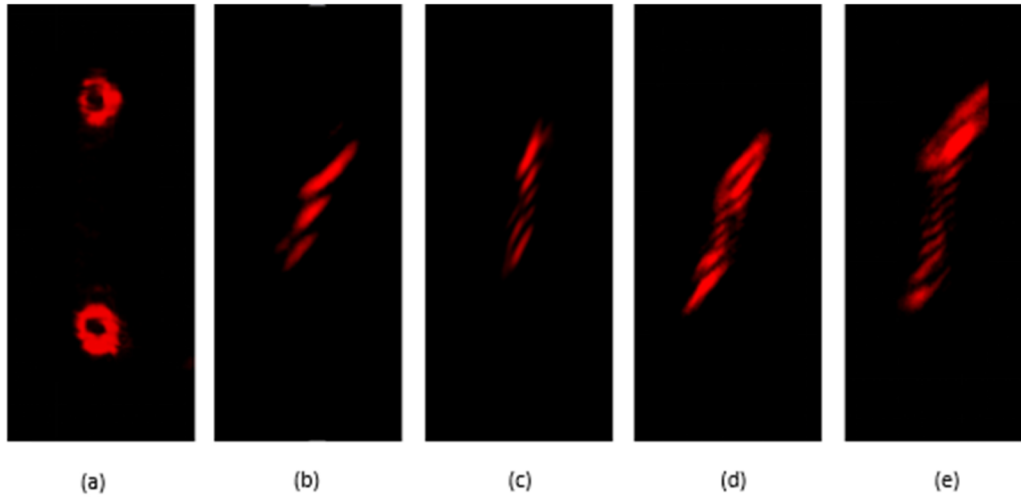


Fig. 3. (a) Image of the second-harmonic-carrying OAM. After using the cylinder lens, converted patterns are obtained for $l_2 = 2, 4, 6,$ and 8 in panels (b–e), respectively.

We then tuned the input wavelength to 1384 nm to achieve THG OAM modes. Behind the sample, the distribution of the second and third harmonics was observed on the screen after filtering out the fundamental beam. There were five donut-shaped spots, which are shown in Fig. 2(b); three are blue and the other two are red, with the red spots located between the blue ones. In the experiment, we separately collected the images of the red spots and blue spots because the former were much stronger than the latter. The observed red spots are similar as the ones shown in Fig. 3(a), which are produced by QPM SHG process with certain phase mismatch (i.e., $\Delta\vec{k}_1 \neq 0$). Although the conversion efficiency of SHG is relatively low, one can still produce substantial second-harmonic waves because the phase mismatch is partially compensated by the reciprocal vector. The second-harmonic beam can participate in the cascaded SFG process, which is well phase-matched (i.e., $\Delta\vec{k}_2 = 0$) at this wavelength. Typical blue spots observed are shown in Fig. 4(a). The upper blue spot in Fig. 4(a) results from the THG through the cascading of the non-collinear SHG process with $\vec{G}_{0,1}$ and the non-collinear SFG process with $\vec{G}_{1,1}$ [Fig. 1(c)]. Similarly, the lower blue spot in Fig. 4(a) is produced by using $\vec{G}_{0,-1}$ for SHG and $\vec{G}_{1,-1}$ for SFG. Interestingly, the middle blue spot in Fig. 4(a) is generated through two cascaded QPM THG configurations: one uses $\vec{G}_{0,1}$ for SHG and $\vec{G}_{1,-1}$ for the cascaded SFG, and the other is its mirror-symmetrical configuration (i.e., $\vec{G}_{0,-1}$ -assisted SHG cascaded with $\vec{G}_{1,1}$ -assisted SFG; Fig. 1(c)). The emission angle of the non-collinear third-harmonic beam is measured to be 6.0° , whereas that of the second-harmonic beam is 4.5° . The theoretical values calculated from Eqs. (4) and (5) are 5.7° and 4.3° for the third- and second-harmonic beams, respectively. The differences between the theoretical and experimental values can be attributed to measurement error and inaccurate dispersion equation.

Through the cylindrical lens, the OAMs of the third-harmonic beam are $l_3 = 3, 6, 9,$ and 12 , which correspond to $l_1 = 1, 2, 3,$ and 4 , respectively [Fig. 4(b)–(e)]. Clearly, the OAM conservation law of $l_3 = 3l_1$ is well established to hold in such cascaded THG processes. The quality of the THG OAM mode in Fig. 4(a) is not perfect because the phase-matching wavelengths of the SHG and SFG processes in our experiment did not completely coincide. If a better NPC structure were designed and fabricated, the mode quality may be further improved.

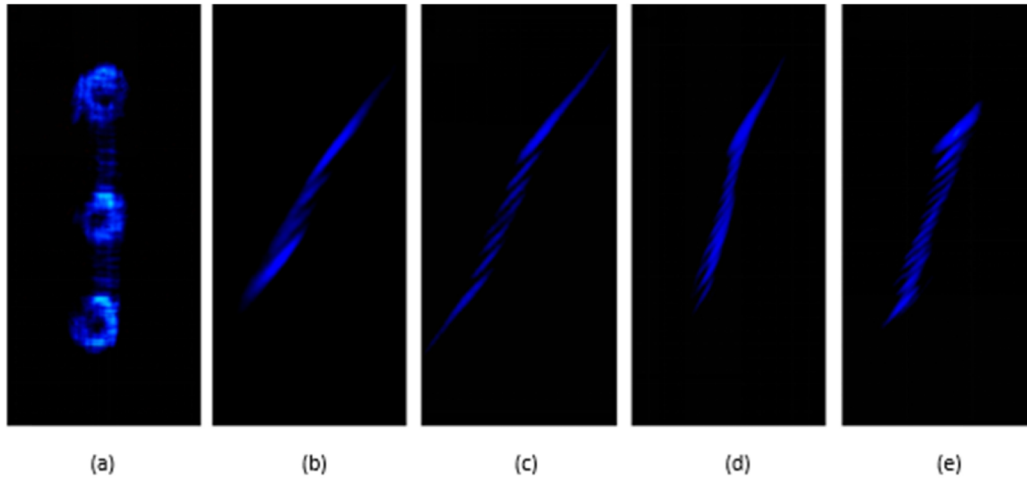


Fig. 4. (a) Image of the OAM-carrying third-harmonic beam. After using the cylinder lens, converted patterns are obtained for $l_3 = 3, 6, 9,$ and 12 in panels (b–e), respectively.

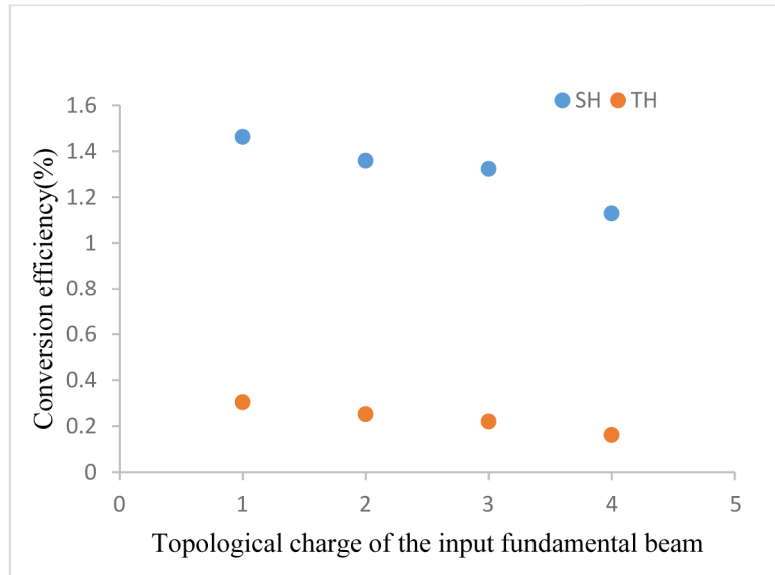


Fig. 5. The conversion efficiencies of SH and TH OAM generations with different input topological charges.

Figure 5 shows the conversion efficiencies of OAM SHG and THG with different input topological charges. The input energy of the fundamental pulse is kept to be 1.5 mJ. We achieved 1.5% conversion efficiency for SHG and 0.3% for THG with an input OAM of $l_1 = 1$. When increasing the input topological charge, the conversion efficiencies of both SHG and THG become lower. This can be explained by the OAM beam shape. For an OAM beam carrying a higher topological charge, the central dark area due to the phase singularity becomes bigger, which results in smaller power density and lower conversion efficiency. In addition, we found that the power dependences of second-harmonic and third-harmonic OAM beams on the fundamental power are similar to that with a Gaussian input beam, i.e., $P_{SH} \propto P_F^2$ and $P_{TH} \propto P_F^3$. Here, P_F , P_{SH} and P_{TH} are powers of the fundamental, second-harmonic and third-harmonic beams, respectively.

4. Conclusion

In conclusion, we experimentally demonstrated OAM conversion through THG in a 2D hexagonally poled LiTaO₃ crystal. THG was achieved by cascading the SHG and SFG processes through a QPM technique. Non-collinear reciprocal vectors play a vital role in compensating the phase mismatch between interacting waves. The OAM conversion law guarantees that the topological charge can be easily doubled or tripled in the SHG or THG process. Such a configuration can be further extended to cascaded high-harmonic generation to produce high topological charges. Our method provides an effective way to obtain multiple high-order OAM modes, which are important for applications in optical communications, imaging, and manipulation.

Funding

National Natural Science Foundation of China (NSFC) (91636106, 11621091, 11674171); National Basic Research Program of China (2016YFA0302500).